Stanford Exploration Project, Report 89, November 12, 1997, pages 1–24

Sediments with gas hydrates: Internal structure from seismic AVO

Christine Ecker, Jack Dvorkin, and Amos Nur[1]

keywords: *velocity, gas, amplitudes, sediment, sandstone, AVO, modeling*

ABSTRACT

We use rock-physics-based synthetic seismic modeling to interpret AVO data of methane hydrate structures. Two micromechanical models of gas hydrate deposition are examined: (1) the hydrate cements grain contacts and strongly reinforces the sediment; and (2) the hydrate is located away from the grain contacts and only weakly affects the stiffness of the sediment's frame. We calculate the effect of pore fluid on seismic velocities from Gassmann's equation. Synthetic seismograms are generated from 1-D elastic modeling (Thompson-Haskell reflectivity method) and the AVO responses at the BSR are obtained from Zoeppritz equations. Comparison with real seismic AVO data from the Blake Outer Ridge, offshore Florida and Georgia, shows that the second model of hydrate deposition can reproduce the real AVO effect qualitatively. The inferred topology of hydrate deposition leads to two important conclusions: (1) the sediment containing hydrate is uncemented and thus mechanically weak, and (2) the permeability of this sediment is very low because hydrate clogs large pore-space conduits. This second conclusion explains the fact that free gas is trapped underneath the BSR at the Blake Outer Ridge. The data furthermore indicate the absence of strong reflections at the top of the hydrate. We conclude that the high concentration of hydrate in the sediment immediately above the BSR gradually decreases with decreasing depth.

INTRODUCTION

Methane hydrate structures are increasingly recognized as both a potential energy resource and a resource that might have a strong "greenhouse" effect on future global climate (Kvenvolden, 1993). Associated with the base of the stability zone of these hydrate structures are so-called bottom simulating reflectors (BSRs) that parallel the seafloor at a subbottom depth of several hundred meters. Knowledge of the elastic and mechanical properties of the hydrate structures and the BSRs is essential to an estimation of the total volume of hydrates in place and its recoverability (permeability

[1]**email:** christin@sep.stanford.edu

and formation strength). The key to extracting these parameters is a combination of seismic analysis and rock physics, which will provide a link between seismic velocity and attenuation and internal rock structure.

Several attempts to obtain the properties of hydrated sediment directly from cores have been thwarted by the instability of methane hydrate at normal temperature and pressure (Kvenvolden and Barnard, 1983; MacKay et al., 1994; Dallimore and Collett, 1995). Consequently, the elastic properties have been inferred from seismic reflection data (Hyndman and Spence, 1992; Singh et al., 1993; Katzman et al., 1994; Ecker and Lumley, 1994). A method of linking these data to the desired properties of hydrated sediment is synthetic forward modeling. Typically, a rock physics hypothesis is used in these models to estimate velocities in hydrate-bearing sediments from those in the sediment frame, and in pure hydrate. The latter two are normally available from ocean-drilling cores and from laboratory measurements (Stoll and Bryan, 1979; Whalley, 1980; Pearson et al., 1986). Dvorkin and Nur (1993) give an example of such a synthetic velocity modeling by assuming that hydrate acts as cement at grain contacts. However, little effort has been done so far to correlate rock physics theory directly with seismic hydrate responses.

This paper is a first attempt to interpret seismic AVO data of hydrate structures by performance of rock-physics-based seismic modeling. We explore the effect of two different hydrate models both on the elastic properties of hydrated sediments and on the seismic responses that can actually be measured. The subsequent link of the modeled internal structure with real seismic data emphasizes one goal of rock physics. This goal is not purely a matching of data by the use of an appropriate theory. Rather it is the at least qualitatively extraction of parameters such as permeability and strength from seismically inferred rock structure.

In this paper, we discuss two mechanical hydrate models, their elastic properties and seismic amplitudes, and the resulting interpretation of AVO data from a bottom simulating reflector (BSR) offshore Florida and Georgia. We examined two micromechanical hydrate models: (1) the hydrate cements the grain contact and strongly reinforces the sediment; and (2) the hydrate is located in away from the grain contacts and only weakly affects the stiffness of the sediment's frame. The hydrate-bearing sediment was brine saturated, while the underlaying sediments contained either brine or free gas. The dry rock properties of model (1) were calculated using the cementation theory by Dvorkin et al. (**?**), while the parameters of model (2) were based on the contact theory of Hertz and Mindlin (1949). Using Gassmann's equation, we determined the saturated elastic rock properties. Synthetic seismograms were generated using the 1-D, elastic Thompson-Haskell reflectivity method. In order to obtain the amplitude behavior at the BSR without interfering converted waves or critical angle effects, we calculated the AVO responses from Zoeppritz equations. A subsequent qualitative comparison of the synthetic results with data from the Blake Outer Ridge, offshore Florida and Georgia, resulted in an interpretation of the in-situ settings in this region.

HYDRATE FORMATION MODELS

Methane hydrates, which can be described as being frozen methane gas, form at the transition of methane through a pressure-temperature dependent phase-boundary. Since the required pressure-temperature conditions usually occur within several hundred meters beneath the seafloor, the sediments above and below the hydrate-bearing sediments can be assumed to be unconsolidated, subjected only to hydrostatic pressure. Depending on the origin of the methane necessary for the hydrate formation, the hydrate-bearing sediments might be underlain by either gas-saturated sediments (Kvenvolden and Barnard, 1983a) or brine-saturated sediments in which the methane saturation does not exceed the saturation solubility of water (Hyndman and Davis, 1992). Several different ways in which the methane then solidifies into hydrate after the transition through the required phase boundary can be imagined. One possibility is that the hydrates formation cements the rock grains together, either by hydrate deposition at the grain contacts or by uniform hydrate deposition on the grain surface, thus considerably increasing the stiffness of the structure (Dvorkin and Nur, 1993). Another possibility might be that the hydrate forms randomly in the pore space without having a direct influence on the rock matrix.

Hydrate formation by cementation (Model 1)

Hydrate formation by cementation describes the mechanical interaction between grains that are bound together by intergranular cement, in this case hydrate (Dvorkin and Nur, 1993). This intergranular cement can be deposited either at the grain contacts or uniformly on the grain surface. A simplified scheme of these depositions can be seen in Figure 1. Since even soft cement is load-bearing (Dvorkin et al., 1991, 1994), only small amounts of cement can significantly increase the stiffness and thus the elastic moduli of granular material and so reduce the porosity. The hydrate not only solidifies, but becomes part of the dry rock frame through its contacts with the grains. Using the theory described by Dvorkin et al. (**?**), we calculate the effective dry elastic moduli of the hydrate-cemented sandstone as

$$K_{eff} = \frac{1}{6}\, n\,(1-\phi_0)\,\rho_h\, {v_{ph}}^2\, S_n \tag{1}$$

$$G_{eff} = \frac{1}{5}\, K_{eff} + \frac{3}{20}\, n\,(1-\phi_0)\,\rho_h\, {v_{sh}}^2\, S_\tau \tag{2}$$

where K_{eff} and G_{eff} are the dry bulk and shear moduli; ρ_h is the density of pure hydrate, v_{ph} its P-wave velocity and v_{sh} its S-wave velocity. ϕ_0 is the initial porosity of the grains before hydrate-saturation, and is the average number of grain contacts for this specific porosity as given by Murphy (1982). The parameters S_n and S_τ are proportional to the normal and shear stiffnesses of a cemented two-grain combination and depend on the amount of the hydrate (cement) and the hydrate and grain properties.

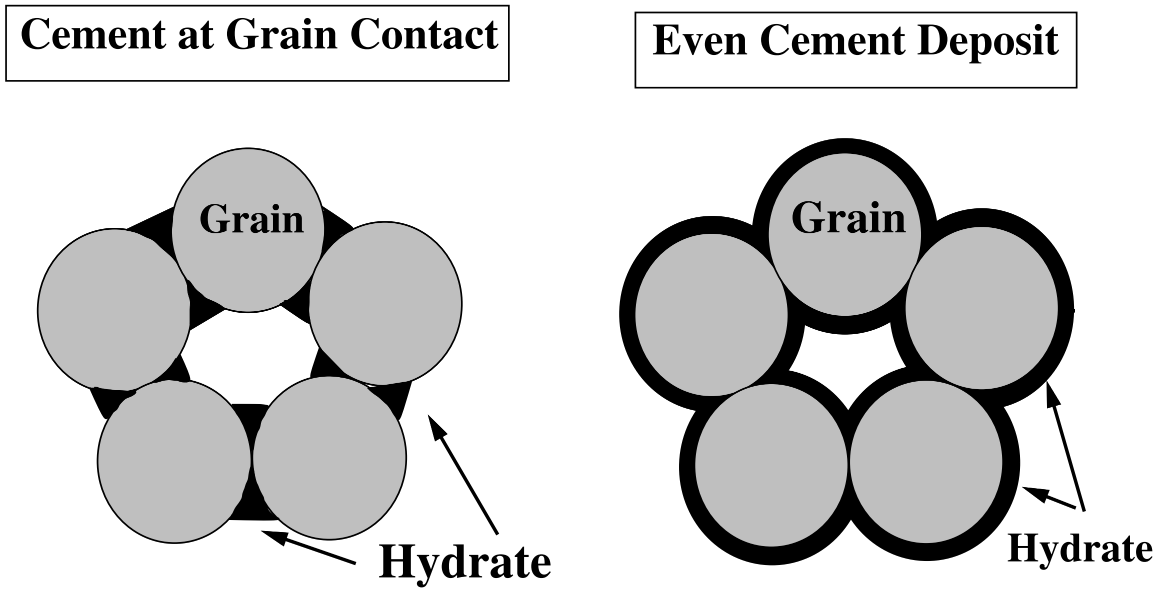

Figure 1: Configuration of the rock after hydrate cementation. christine1-cement.pore [NR]

The amount of hydrate α depends on the way the hydrate is distributed along the grains. In the case where it is deposited only at the grain contact,

$$\alpha = 2 \left(\frac{S\, \phi_0}{3\, n\, (1 - \phi_0)} \right)^{0.25} \tag{3}$$

while for a uniform hydrate deposition,

$$\alpha = \left(\frac{2\, S\, \phi_0}{3\, (1 - \phi_0)} \right)^{0.5} \tag{4}$$

where S is the hydrate saturation of the pore space.

Hydrate formation only in the pores (Model 2)

Another possible means of hydrate formation might be the solidification of the methane in the pore space only, away from the grain contacts (Figure 2). In this case the hydrate is solidified, but does not become part of the dry rock matrix by cementation. The rock grains are held together only by the effect of the confining pressure. An increase in stiffness would result only at considerable hydrate saturation of the pore space, in contrast to the previously-described cementation case. The effective dry moduli of the hydrate-bearing sandstone at critical porosity $\phi_c = 0.36$ can be described by the Hertz-Mindlin contact theory (Mindlin, 1949):

$$K_{HM} = \left(\frac{n^2 \, (1-\phi_c)^2 \, G^2}{18 \, \pi \, (1-\nu)^2 \, P} \right)^{\frac{1}{3}} \tag{5}$$

$$G_{HM} = \frac{5 \; - \; 4 \, \nu}{5 \, (2-\nu)} \left(\frac{3 \, n^2 \, (1-\phi_c)^2 \, G^2}{2 \, \pi \, (1-\nu)^2 \, P} \right)^{\frac{1}{3}} \tag{6}$$

where ν is the grain Poisson's ratio, G is the grain shear moduli and P is the confining pressure.

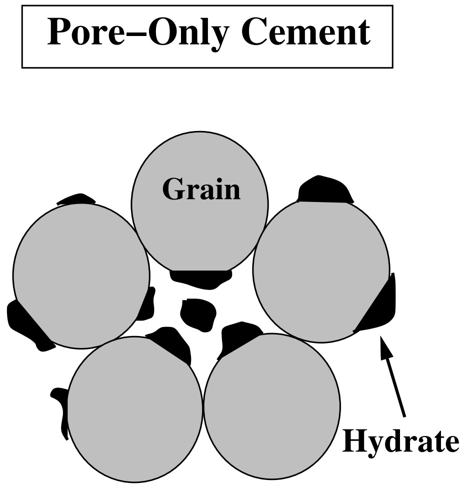

Figure 2: Configuration of the rock matrix after deposition of the hydrate as pore-only cement. christine1-nocement.pore [NR]

In order to calculate the effective dry moduli at a different porosity, we used the heuristically modified Hashin-Strikman lower bound proposed by Dvorkin and Nur (1995):

$$K_{eff} = \left(\frac{\phi_0/\phi_c}{K_{HM} \, + \, \frac{4}{3} \, G_{HM}} + \frac{1 \; - \; \phi_0/\phi_c}{K \; + \; \frac{4}{3} G_{HM}} \right)^{-1} - \frac{4}{3} \, G_{HM} \tag{7}$$

$$G_{eff} = \left(\frac{\phi_0 \, / \, \phi_c}{G_{HM} + \frac{G_{HM}}{6} \left(\frac{9 \, K_{HM} + 8 \, G_{HM}}{K_{HM} + 2 \, G_{HM}} \right)} + \frac{1-\phi_0 \, / \, \phi_c}{G + \frac{G_{HM}}{6} \left(\frac{9 \, K_{HM} + 8 \, G_{HM}}{K_{HM} + 2 \, G_{HM}} \right)} \right)^{-1} - \frac{G_{HM}}{6} \left(\frac{9 \, K_{HM} + 8 \, G_{HM}}{K_{HM} + 2 \, G_{HM}} \right) \tag{8}$$

where K is the grain bulk modulus, and ϕ_0 is the original porosity of the grains.

Saturated elastic moduli for Model 1 and Model 2

The effective dry moduli of the different hydrate frameworks have to be related to the effective moduli of the same rock-containing fluid. The effective moduli of a saturated rock can be calculated at seismic frequencies by means of Gassmann's formulas:

$$\frac{K_{sat}}{K_{solid} - K_{sat}} = \frac{K_{dry}}{K_{solid} - K_{dry}} + \frac{K_{fluid}}{\phi\,(K_{solid} - K_{fluid})} \tag{9}$$

$$G_{sat} = G_{dry} \tag{10}$$

where K_{sat} and G_{sat} are the effective bulk and shear moduli of the saturated rock; K_{dry} and G_{dry} the moduli of the dry rock; K_{fluid} and G_{fluid} the moduli of the fluid; and K_{solid} the bulk modulus of the mineral material making up the rock. ϕ is the porosity of the saturated rock.

The effective moduli of the mineral K_{solid} can be calculated using the Voigt-Reuss-Hill average, which is an arithmetic average of the Voigt upper bound (K_V) and the Reuss lower bound (K_R):

$$K_{solid} = \frac{K_V + K_R}{2} \tag{11}$$

with

$$K_V = f\,K + f_h\,K_h \tag{12}$$

$$\frac{1}{K_R} = \frac{f}{K} + \frac{f_h}{K_h} \tag{13}$$

where f and f_h are the volume fractions of the grains and the hydrate, respectively. K is the grain bulk modulus and K_h is the hydrate bulk modulus.

In order to calculate the effective fluid bulk modulus K_{fluid} for partially-saturated rocks, we used the following equation:

$$\frac{1}{K_{fluid}} = \sum_{i=1}^{N} \frac{f_i}{K_{fluid_i}} \tag{14}$$

where f_i is the volume fraction of the fluid, N is the number of fluids, and K_{fluid_i} is the bulk modulus of the fluid.

After having derived the effective moduli of the saturated rock, we used the following relationships to find the seismic velocities in saturated rock:

$$v_{p_{sat}} = \sqrt{\frac{K_{sat} + \frac{4}{3}\,G_{sat}}{\rho_{sat}}} \tag{15}$$

$$v_{s_{sat}} = \sqrt{\frac{G_{sat}}{\rho_{sat}}} \tag{16}$$

where ρ_{sat} is the density of the saturated rock,

$$\rho_{sat} = (1-\phi)\,\rho_{solid} + \phi\,\rho_{fluid} \tag{17}$$

ρ_{solid} is the density of the solid phase, and ρ_{fluid} is the density of the fluid phase which can be obtained from:

$$\rho_{fluid} = \sum_{i=1}^{N} f_i \rho_{fluid_i} \tag{18}$$

Velocity behavior of Model 1 and Model 2

Using the relationships between dry, solid, and saturated elastic moduli that were defined in the previous sections, we calculate the P- and S-wave velocities of Model 1 and Model 2 for different hydrate saturations. We assume a basic and simple rock model consisting of pure, high-porosity ($\approx 30\%$) sandstone subjected to a confining pressure of 10 MPa. Since the hydrates usually form at a subbottom depth of only several hundred meters, these conditions resemble the in-situ conditions. To simulate hydrate formation, we calculated the effective dry moduli of the hydrate layer with the help of either both equations (1) and (2) or equations (5) through (8). The saturated velocities are again obtained from equations (9) through (18). The sediment underlaying the hydrated sediment is saturated by either 100% water or a water-gas mixture, depending on the origin of the methane. Assuming that this sediment is unconsolidated, its dry moduli are calculated using the Herz-Mindlin contact theory as described by equations (5) through (8). Subsequently, equations (9) through (18) are used to determine the effective bulk moduli after brine or gas saturation and to estimate the corresponding P-wave and S-wave velocities. The properties of the quartz, pure hydrate, water, and gas used for these simulations are listed in Table 1.

substance	K [MPa]	μ [MPa]	ρ [kg/m^3]	v_p [m/s]	v_s m/s]
quartz	36600	45000	2650	6037	4121
water	2250	0	1000	1500	0
pure hydrate	5600	2400	767	3450	1769
gas	10	0	100	375	0

Table 1: Properties of water, gas, pure hydrate and quartz

Figure 3 shows the velocity behavior of the hydrate-bearing sandstones for different hydrate saturations. These are compared with the velocities Vp and Vs of sandstone with different gas saturation in order to create a visualization of the change in properties at the transition to hydrate-bearing sediment.

It is obvious that the velocity behavior in the case where the hydrate was deposited at the grain contacts and in the case where it was deposited uniformly on the grain surface is very similar. In both cases, merely small amounts of hydrate saturation increase the P- and S-wave velocities considerably compared to brine and gas-saturated sandstone. The more hydrate is deposited, the stiffer the rock becomes, and the faster are its P- and S-wave velocities. This effect is even more evident for hydrate deposition at the grain contacts than it is for the uniform hydrate deposition on the grain surface.

The solidification of the hydrate in the pore-space only, on the other hand, affects the velocities in a slightly different way. Small amounts of hydrate deposition cause a negligibly, small increase of the P-wave velocity with regard to brine-saturated sandstone, and do not cause any change at all in the S-wave velocity. To obtain a noticeable increase in the P-wave velocity, a significant ($> 15\%$ by volume) amount of hydrate has to deposited. Even then, there is barely a change in the S-wave velocity. Since deposition in the pore space does not immediately affect the stiffness of the rock, this velocity behavior can be expected. Comparison of the velocities with those of gas-saturated sandstone shows an increase in the P-wave velocity and a slight decrease in the S-wave velocity.

The increase in P-wave velocity in all three models agrees well with seismic velocity analyses of in-situ BSRs (Hyndman and Spence, 1992; Singh et al., 1993; Katzman et al., 1994; Ecker and Lumley, 1994). While a sufficient increase can be obtained with only a small amount of hydrate in the cementation models, the pore-only deposition model requires a considerable amount of hydrate to be present in order to obtain the same P-wave velocity increase. Since the P-wave velocities alone cannot discriminate between the unique models, the S-wave velocities in the hydrate structures are of importance. Since the S-wave velocity behavior is different depending on hydrate cementation or merely on deposition in the pore space, seismic AVO analysis should be a good indicator of the deposition structure found in-situ.

AVO ANALYSIS

In order to evaluate the effects of the different hydrate deposition models on seismic reflection responses, we performed 1-D, elastic modeling using the Thompson-Haskell reflectivity method. All layers were assumed to be flat and approximately 300 meters thick. We used the previously-calculated, saturated velocities of the different hydrate models as input for the hydrate-saturated layer. The hydrate layer was overlain by a brine-saturated sandstone and underlain by either a brine-saturated sandstone layer or a gas-saturated sandstone layer. For the gas-saturated sandstone layer we chose a 50%

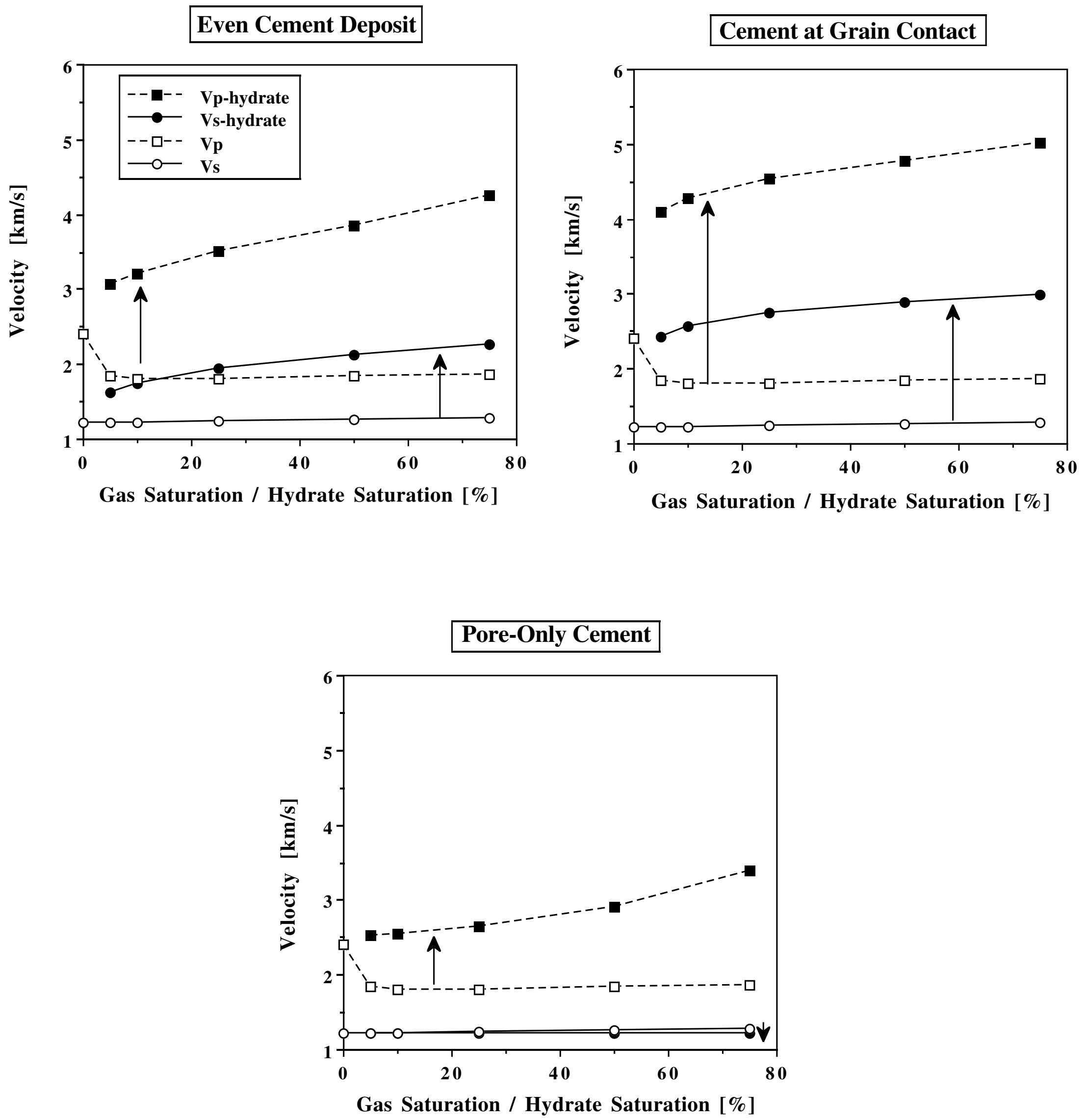

Figure 3: Velocity behavior of the different hydrate deposition theories for different hydrate saturations. These velocities (Vp-hydrate and Vs-hydrate) are compared with the velocities of sandstone (Vp and Vs), which is saturated with different amounts of gas. christine1-cement [NR]

gas saturation. The properties of theses layers were also calculated in the previous section (Figure 3). The configuration of the two different synthetic models, one model simulating the structure for hydrate overlaying brine, one simulating hydrate overlaying gas, can be seen in Figure 4. Both models were overlain by a thick water column.

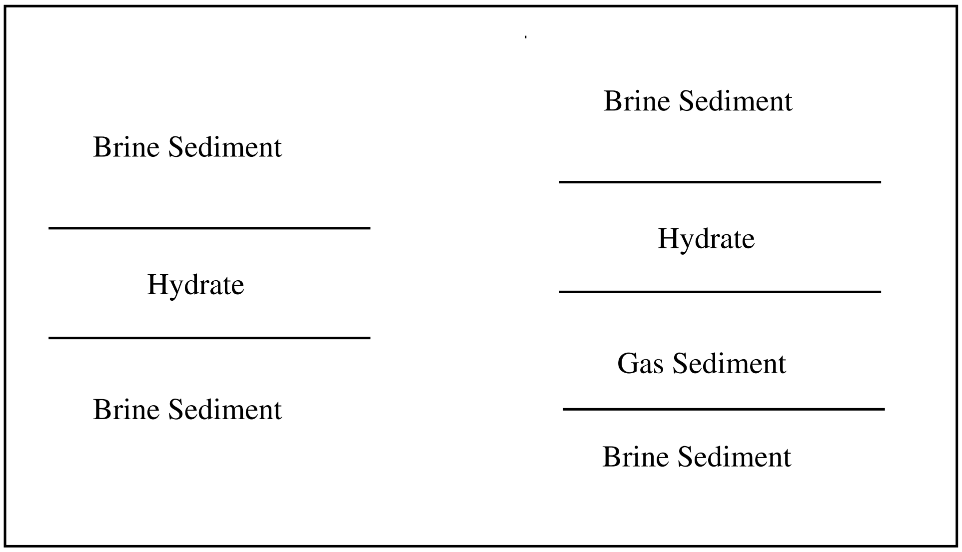

Figure 4: Synthetic models for the hydrate structures. The left model shows the configuration for hydrate overlaying brine, the right shows hydrate over gas. christine1-model [NR]

We generated synthetic seismograms for different hydrate saturation in the hydrate layer and compared the different seismic responses. Subsequently, in order to evaluate the actual amplitude behavior at the BSR, which is the bottom of the hydrate stability zone, we determined its AVO response using Zoeppritz equations.

Hydrate deposition by cementation (Model 1)

First, we modeled the seismic responses of the hydrate-cemented structures. Since the velocity behavior of both cementation possibilities behave in the same way, we chose only the case of uniformly-deposited hydrate on the grain surface for the seismic modeling. Any amplitude responses from the top and bottom of the hydrate layer should be even more pronounced in the case of cementation at the grain contacts, since the velocities in this case are even higher.

Figure 5 shows the synthetic seismograms for different hydrate saturations in the case where the hydrate-bearing sandstone is underlain by brine-saturated sandstone. Both the top and the bottom of the hydrate layer (BSR) produce clear reflections. Since the hydrate layer represents a high velocity zone, the reflection at the BSR, the bottom of the hydrate zone, shows a reversal in polarity. Such a polarity change is frequently associated with BSRs recorded in real seismograms. The near-offset amplitudes from the top and bottom have approximately comparable strength. While the top of the hydrate zone displays a clear increase of amplitude with offset, the BSR response diminishes with increasing offset, and is in fact barely visible there. The higher the hydrate saturation in the layer, the higher the velocity contrast between the hydrate layer and the brine layers, and, consequently, the stronger the reflections from the top and the bottom. Considering that in reality the seismograms are contaminated with noise, the responses of the layer for small amounts of hydrate saturation appears to be too weak to be visible. It is, furthermore, obvious that a large amount of converted waves interfere with the primary signals.

In the case where the hydrate-bearing sandstone is underlain by gas-saturated sandstone, the synthetic modeling results in the seismograms shown in Figure 6. As before, the seismograms display clear reflections from the top and the bottom of the hydrate layer and, additionally, from the bottom of the gas layer. The BSR reflection again has reversed polarity, but appears to have stronger amplitudes than before. This is because there is already a significant velocity contrast for small hydrate saturations. A gas layer has considerably smaller P-wave velocity than a brine layer, thus increasing the P-wave velocity contrast at the BSR. Therefore, the amplitudes at the BSR at the near-offset appear to be stronger than those at the top of the hydrate and the bottom of the gas. As before, the BSR amplitudes decrease with increasing offset.

Both the hydrate-over-brine and the hydrate-over-gas cases show clear reflection signals from the top of the hydrate, that increase with increasing hydrate saturation. In reality, no clear top of the hydrate zone has so far been resolved in seismic sections. This indicates that the hydrate layer has to be a gradual accumulation of hydrate with small amounts of hydrate at the top. Otherwise, the top of the hydrate would result in clear signals visible in seismograms.

In order to determine the amplitude behavior at the BSR without interfering converted wave or critical angle effects, we calculated the AVO response using Zoeppritz equations. Figure 7 shows the results for hydrate sediment overlaying brine-saturated sandstone and hydrate sediment overlaying gas-saturated sandstone.

It is obvious that in both cases the amplitudes present a clear AVO trend that decreases with increasing offset. The zero-offset reflection amplitude mainly depends on the P-wave velocity contrast between the hydrate and the underlaying sandstone and becomes stronger with increasing velocity contrast. Since the contrast is considerably more pronounced in the case of gas-saturated sandstone, the zero-offset amplitudes in that case are significantly higher. The trend of the amplitudes with increasing offset is solely controlled by the S-wave velocity contrast, since there is no significant change in the density at the transition from hydrate to either brine or gas sandstone. The considerable increase in S-wave velocity compared to that in brine and in gas sandstone causes the amplitudes to decrease with increasing offset.

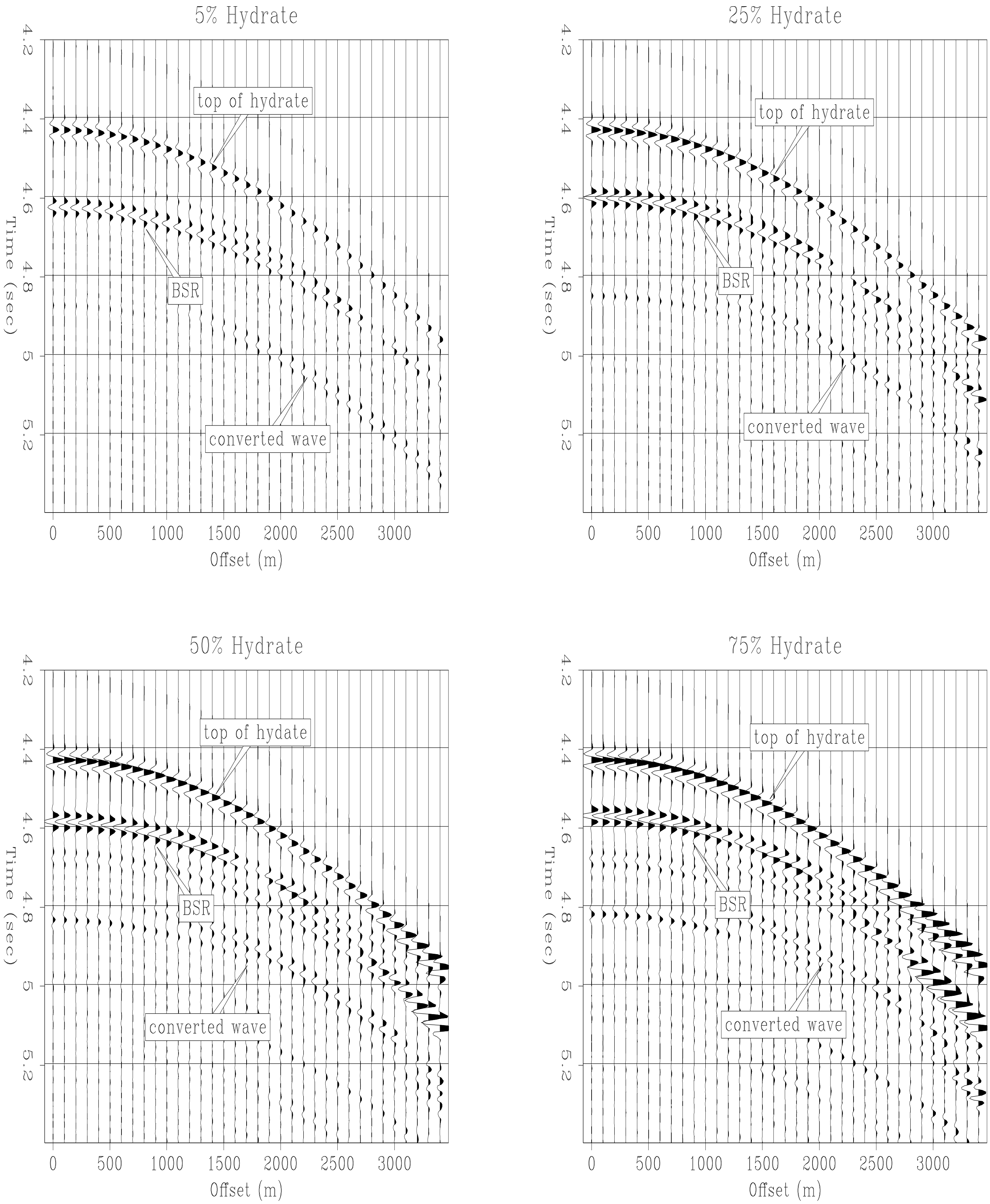

Figure 5: Synthetic seismograms for a cemented hydrate structure containing different amounts of hydrate saturation overlaying brine-saturated sandstone. christine1-cem.brine.ann [CR]

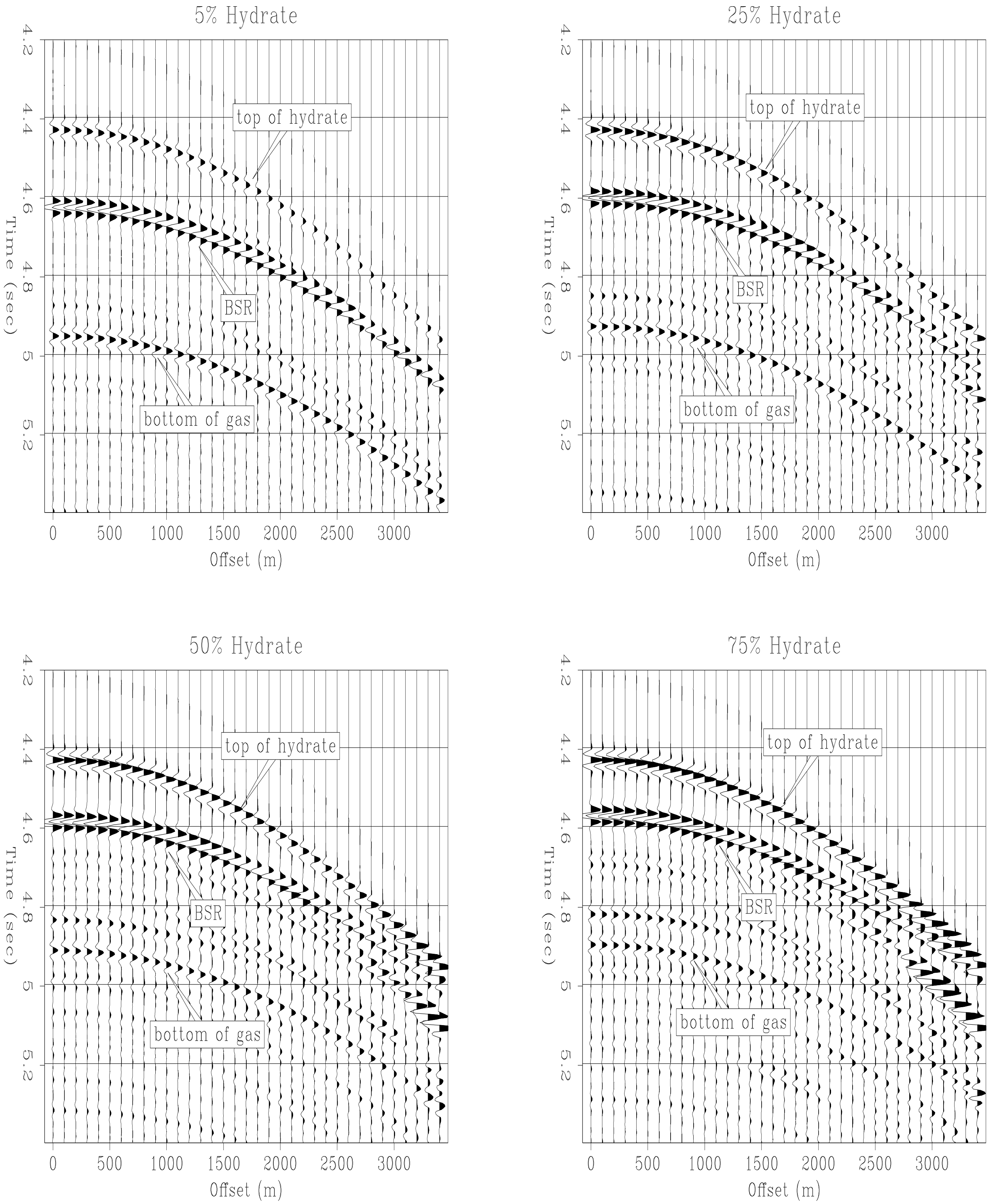

Figure 6: Synthetic seismograms for a cemented hydrate structure containing different amounts of hydrate saturation overlaying gas-saturated sandstone. christine1-cem.gas.ann [CR]

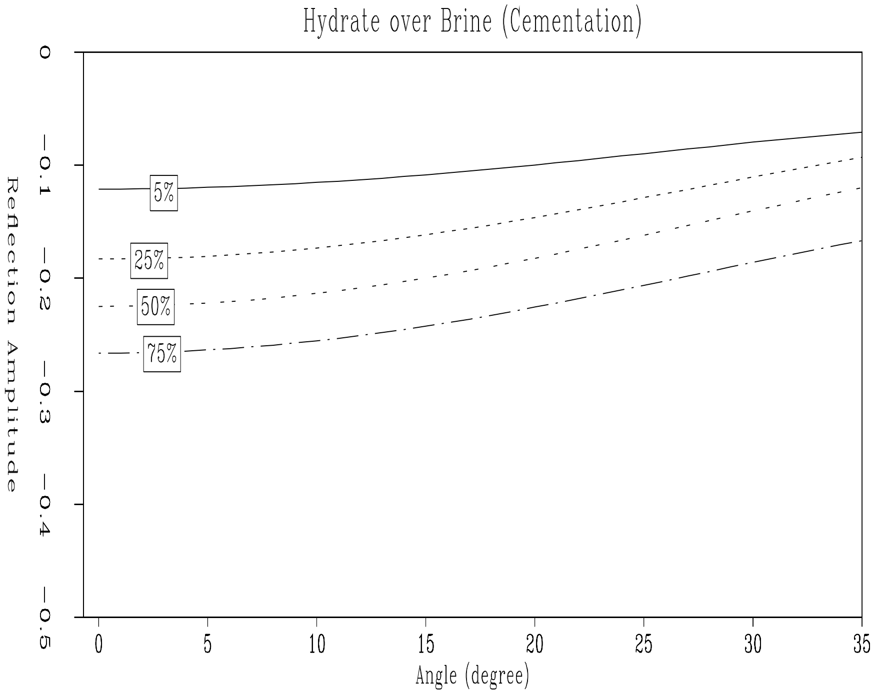

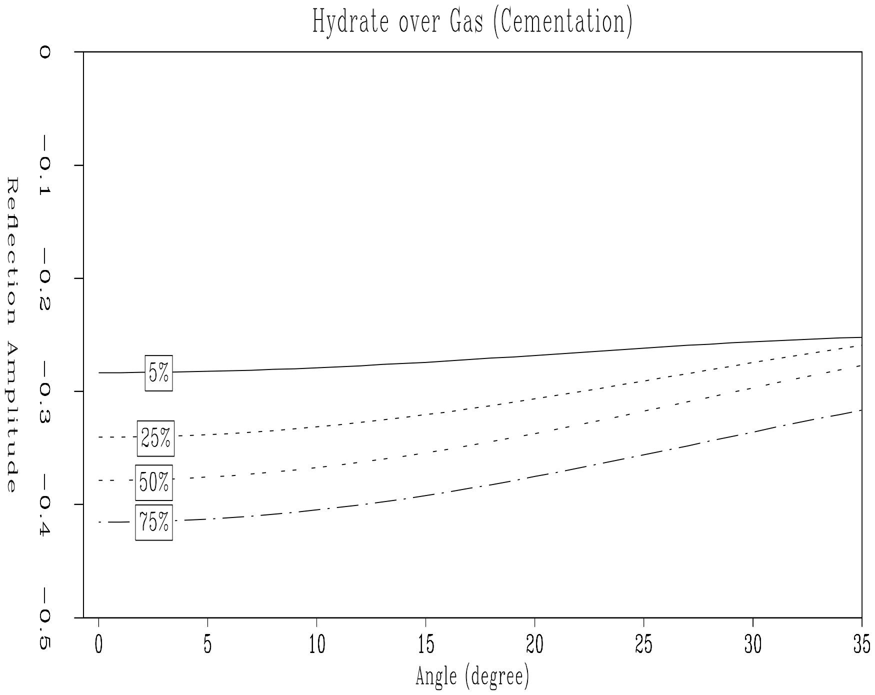

Figure 7: Calculated AVO responses at the BSR for different hydrate saturations in the case of hydrate cementation. The upper panel shows the amplitude behavior for hydrate overlaying brine, while the lower panel shows the amplitudes for hydrate over gas. christine1-avo.cement [ER]

Hydrate deposition in the pores only (Model 2)

After evaluating the effect of hydrate cementation on the seismic amplitudes and reflection responses, we performed the same modeling procedure for the case of hydrate deposition in the pore space only. As before, we modeled two cases. In one case, the hydrate is overlaying brine-saturated sandstone, while in the other case the hydrate is overlaying gas-saturated sandstone.

Figure 8 shows the synthetic seismograms for different hydrate saturations in the case where the hydrate is underlain by brine sandstone. The reflection signals are caused by the top and the bottom of the hydrate zone. As described in the previous section, the signal at the BSR has reversed polarity, and the amplitudes of the reflectors become stronger with increasing hydrate saturation. Since small amounts of hydrate saturation do not affect the velocities significantly, there are barely reflection signals for hydrate saturations less than 50%. Considering noise contamination in real seismograms, these signals would not be visible. For hydrate saturations more than 50%, the top and bottom show strong amplitudes. The BSR signal appears to increase slightly with increasing offset.

Figure 9 illustrates the synthetic seismograms resulting in the case where the hydrate-bearing sandstone is overlaying gas-saturated sandstone. The visible reflections are again caused by the top and bottom of the hydrate and additionally by the bottom of the gas layer. In contrast to the case of brine saturation, the BSR already displays strong reflection amplitudes for only small amounts of hydrate saturation. This is caused by the higher velocity contrast between hydrate and gas-saturated sandstone. The top of the hydrate results, as before, in small reflection amplitudes for small hydrate saturation and increasing amplitudes with increasing saturation. For hydrate saturations less than 50% these amplitudes are in fact barely visible and would not be resolved in reality. The amplitudes at the BSR appear to be increasing with increasing offsets.

We again used Zoeppritz equations to calculate the actual AVO responses at the BSR and to compare them with each other. The results can be seen in Figure 10. The upper panel shows the amplitude behavior for hydrate overlaying brine sandstone, the lower panel shows the amplitudes resulting from hydrate overlaying gas-saturated sandstone.

It is obvious that the amplitude behavior in both cases is opposite to the amplitude behavior displayed when the hydrates were deposited as cement. The relatively small zero-offset reflection amplitudes for hydrate overlaying brine reflect the absence of a significant P-wave velocity contrast in this case. The amplitude trend shows increasingly negative amplitudes with increasing offset. Since the S-wave velocity in the hydrate decreases only slightly relative to the one in brine with increasing hydrate saturation, we can attribute this effect mainly to the P-wave velocity contrast. For only small amounts of hydrate saturation, the increase in amplitude is relatively small. It becomes more pronounced the more hydrate is present in the hydrate layer. In the case where the hydrate is overlaying gas-saturated sediment, the zero-offset re-

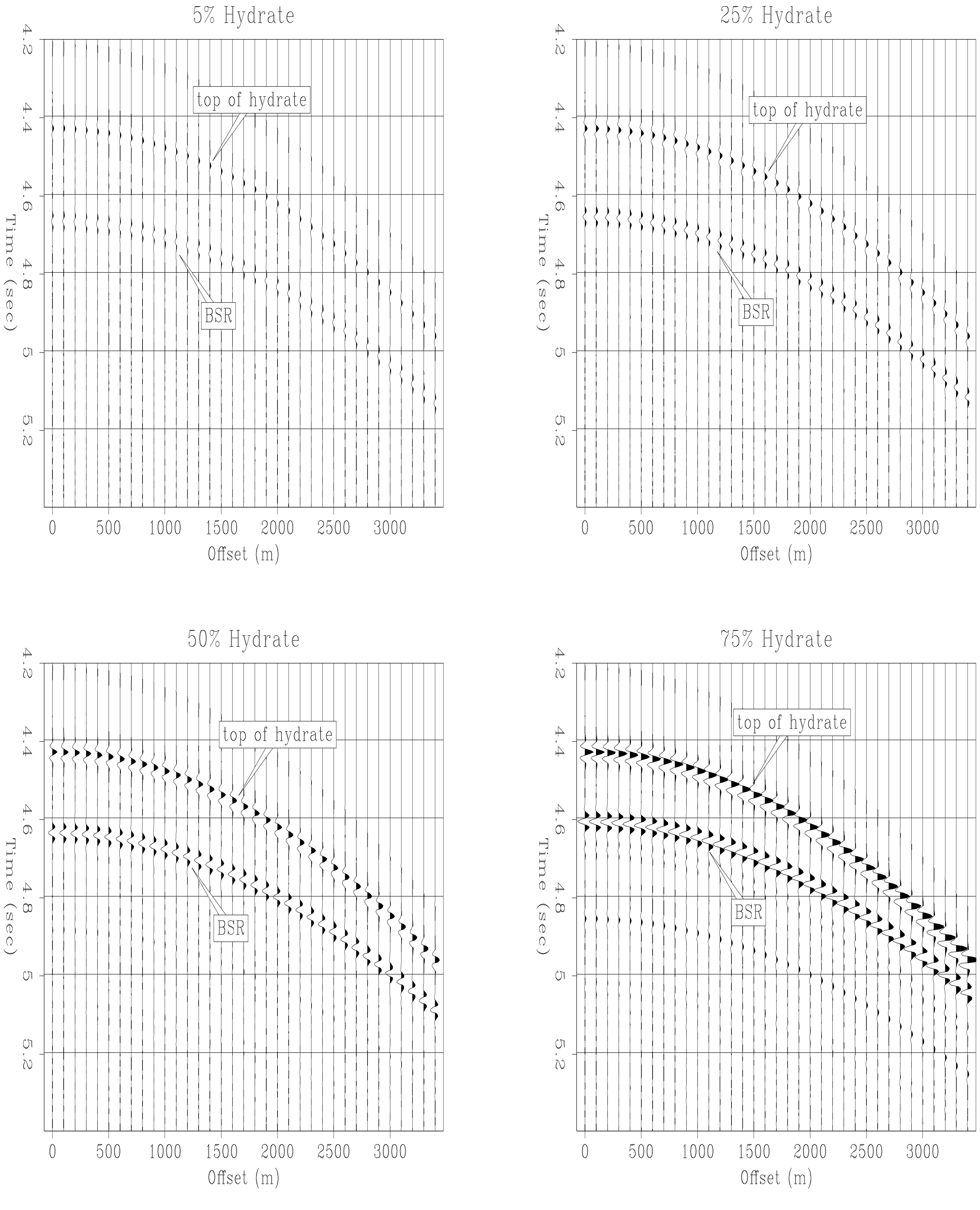

Figure 8: Synthetic seismograms for hydrate deposited in the pores with different hydrate saturations overlaying brine-saturated sandstone. christine1-nocem.brine.ann [CR]

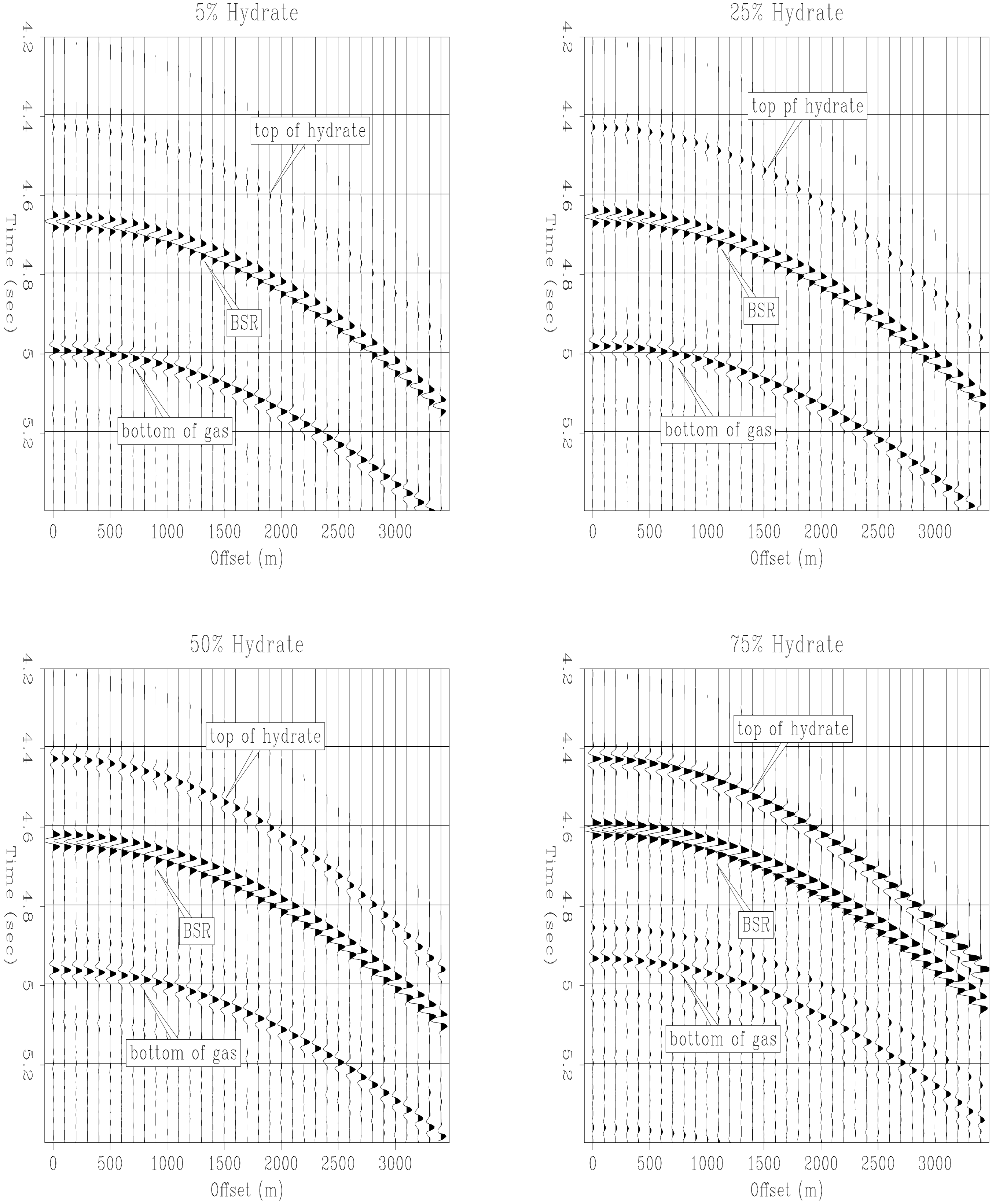

Figure 9: Synthetic seismograms for hydrate deposition in the pore space with different amounts of hydrate saturation overlaying gas-saturated sandstone. christine1-nocem.gas.ann [CR]

flection amplitude is higher. Furthermore, only small amounts of hydrate saturation have a stronger effect on the AVO response.

It will be difficult to discriminate between sediment containing a significant amount of hydrate overlaying brine sediment and sediment containing only a small amount of hydrate overlaying gas sediment from the reflection responses alone. Additional information from seismic velocity analysis, on the other hand, should make such a distinction possible.

REAL DATA COMPARISON

In the preceding section, we have determined the AVO behavior of two micromechanical models of hydrate deposition. We can now link the modeled internal hydrate structure with real seismic data from the Blake Outer Ridge, offshore Florida and Georgia. Since we assumed a very basic rock model in the rock-physics-based seismic modeling, we do not try to match the data quantitatively, but attempt to extract qualitatively parameters such as permeability and strength from the seismically-inferred rock structure.

Figure 11 shows seismic data from a hydrate deposit at the Blake Outer Ridge. The upper panel is an actual CMP gather containing the reflections of the seafloor, the BSR, and a “flat” reflector, probably the transition from gas to brine sediment (Ecker and Lumley, 1994). Above the BSR, there is a “quiet zone” where no reflections are visible. This might be caused by the presence of disseminated methane hydrate. It is obvious from the seismogram that there is no strong reflection visible from the top of the hydrate, while there seems to be a clear reflection from the bottom of the gas-saturated sediment layer. The lower panel compares the amplitude picked along the BSR with the theoretically calculated trend using Zoeppritz equations. The amplitudes display a significant increase of amplitudes with increasing offset. Performing a detailed velocity and AVO analysis, Ecker and Lumley (1994) showed that this behavior is compatible with hydrate overlaying gas-saturated sediment. The P-wave velocity above the BSR is significantly larger than that below the BSR, while the S-wave velocity above the BSR is smaller than that below the BSR.

We have seen in the previous section that hydrate cementation results in a decrease of amplitudes with increasing offset. Even though this model can explain the sharp reflection at the BSR and the muting of lithology contrast above the BSR, it cannot explain the real AVO data.

Hydrate deposition within the pore space, however, seems to qualitatively reproduce the observed AVO effect (Figure 10). In this model the hydrate is located away from the grain contacts and thus only weakly affects the stiffness of the sediment frame. The qualitative fit of the in-situ seismic hydrate response with this rock physics model means that: (1) the hydrated sediment is mechanically weak because the grains are not cemented, and (2) the permeability is small (as compared to the cementation case) because the large pore-space conduits are blocked by the hydrate.

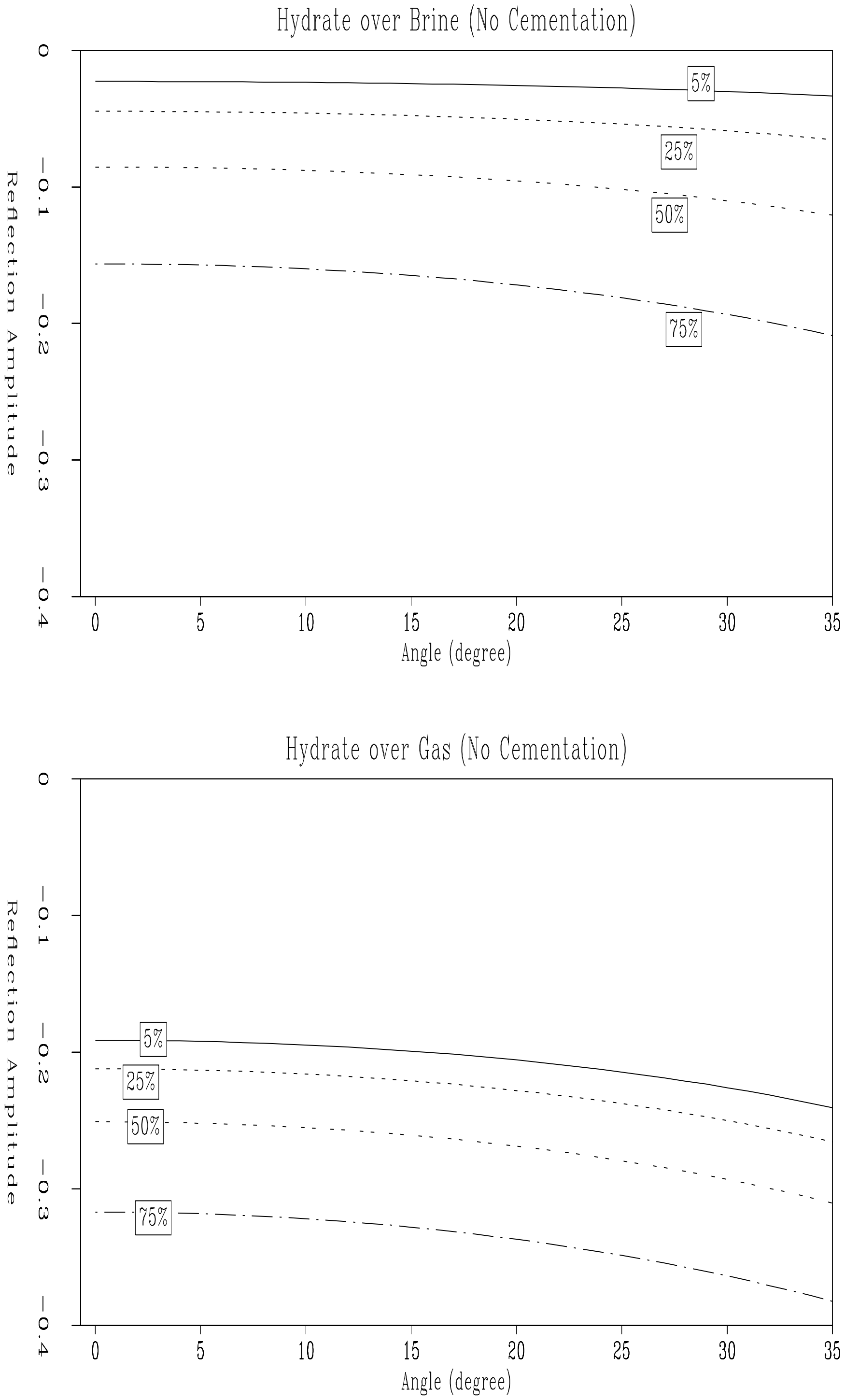

Figure 10: Calculated AVO response at the BSR for the deposition of hydrate in the pores only, depending on different amounts of hydrate saturation. The upper panel shows the amplitudes for hydrate over brine, while the lower panels displays the amplitude behavior for hydrate over gas. christine1-avo.nocement [ER]

The latter explains why free gas is trapped underneath the BSR at the Blake Outer Ridge. The fact that the hydrate in this region is underlain by gas-saturated sediment was shown by Ecker and Lumley (1994). Furthermore, significant amounts of hydrate appear to be necessary in the sediment in order to obtain a strong BSR reflection. The data also indicates the absence of a strong reflection from the top of the hydrated sediment. Based on the synthetic modeling of the previous sections, we conclude that the high concentration of hydrate in the sediment just above the BSR gradually decreases with decreasing depth. This means the hydrate is accumulated immediately above the BSR and dissolves further away from the BSR.

Although the hydrate deposition within the pore space can reproduce the data well in a qualitative way, it cannot do so quantitatively. In order to achieve this, we need to assume a more complex grain substance than pure quartz for the rock matrix. Since there is a high amount of clay present in the sediments in the region of the Blake Outer Ridge, its effect on the elastic moduli will have to be determined. However, the use of the simple model already lets us extract information about crucial parameters such as permeability and strength.

CONCLUSIONS

We evaluated three different forms of hydrate deposition in the pore space, their effect on the elastic properties of hydrate structures and their resulting AVO responses.

The analysis suggests that already small amounts of hydrate cementation result in a significant increase of both the P- and S-wave velocity compared to the velocities of either brine- or gas-saturated sandstone. The cementation caused an immediate stiffening of the rock. Consequently, the synthetic seismograms displayed an AVO effect at the bottom of the hydrate zone that was decreasing with increasing offset. The opposite behavior was observed for the hydrate deposition in the pore space. Strong P-wave velocity contrasts could only be reached by high hydrate saturation. There was barely a change in S-wave velocity at small hydrate saturations, while the S-wave velocity decreased with increasing hydrate saturation. This velocity behavior resulted in an increase of reflection amplitude with increasing offset at the BSR. Both models showed that in case where the hydrate overlays brine sediment, the overall reflection amplitudes are significantly smaller than that in which the hydrate overlays gas sediment.

Comparison of the synthetic results with real in-situ observations at the Blake Outer Ridge showed that the hydrate cementation model cannot sufficiently recreate the amplitude behavior. However, the deposition of hydrate in the pores appears to create an amplitude behavior that can be observed in reality. This leads to two important conclusions about in-situ hydrate structures at the Blake Outer Ridge: (1) the sediment containing hydrate is uncemented and thus mechanically weak, and (2) the permeability of this sediment is very low because hydrate clogs large pore-space conduits, which explains the presence of free gas underneath the hydrate layer at the

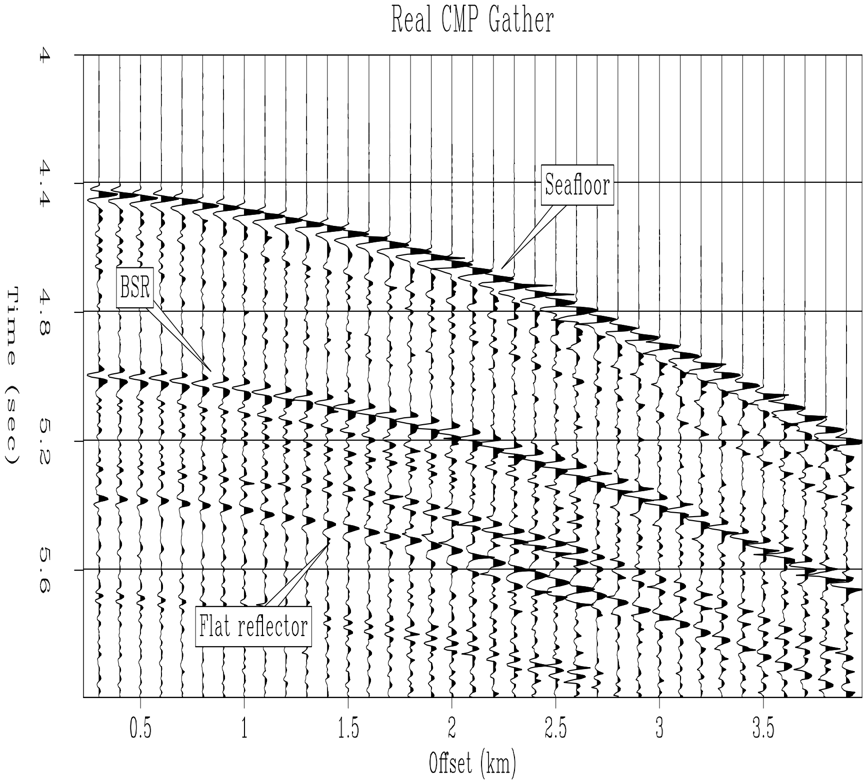

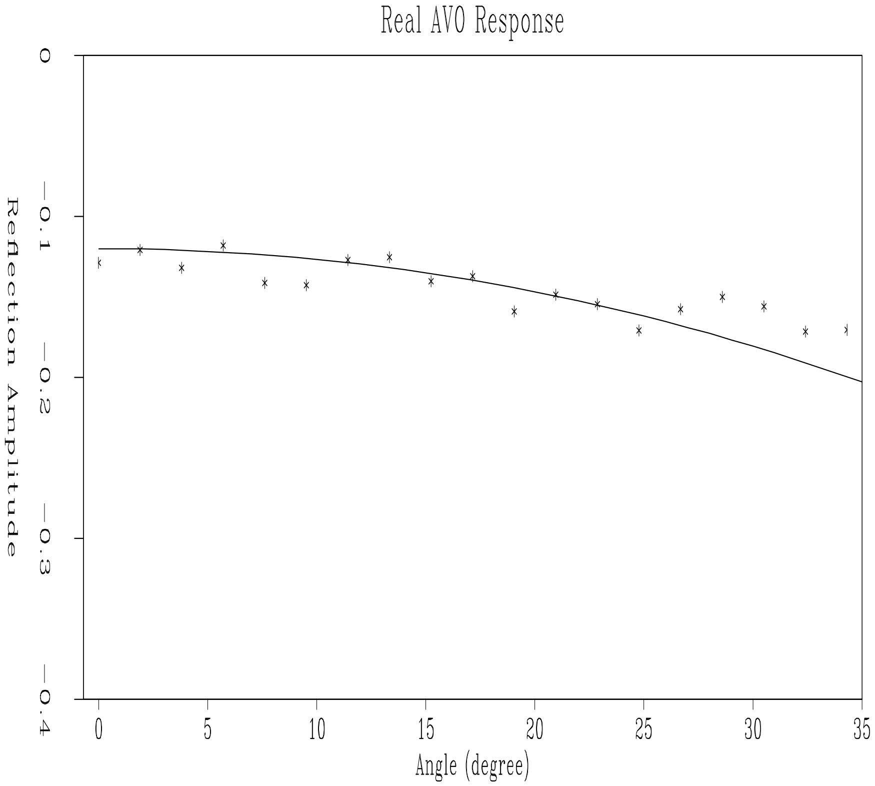

Figure 11: Data from the Blake Outer Ridge, offshore Florida and Georgia. The upper panel shows a CMP gather. The lower panel displays the amplitude picks along the BSR and their theoretical matches calculated using Zoeppritz equations. christine1-real [ER]

Blake Outer . Furthermore, the real data indicate the absence of a strong reflection at the top of the hydrate. We conclude that the high concentration of hydrate in the sediment immediately above the BSR gradually decreases with decreasing depth.

REFERENCES

Dallimore, S. R., and Collett, T. S., 1995, Intrapermafrost gas hydrates from a deep core hole in the Mackenzie Delta, Northwest Territories, Canada: Geology, **23**, 527–530.

Dvorkin, J., and Nur, A., 1993, Rock physics for characterization of gas hydrates: The Future of Energy Gases, U.S. Geol. Survey Professional Paper 1570, pages 293–298.

Dvorkin, J., and Nur, A., 1995, Elasticity of high-porosity sandstones: Theory for two North Sea datasets: Geophysics, submitted.

Dvorkin, J., Mavko, G., and Nur, A., 1991, The effect of cementation on the elastic properties of granular material: Mechanics of Materials, **12**, 207–217.

Dvorkin, J., Nur, A., and Yin, H., 1994, Effective properties of cemented granular material: Mechanics of Materials, **18**, 351–366.

Ecker, C., and Lumley, D. E., 1994, Seismic AVO analysis of methane hydrate structures: 64th Ann. Internat. Meeting, Soc. Expl. Geophys., Expanded Abstracts, 1100–1103.

Hyndman, R., and Davis, E., 1992, A mechanism for the formation of methane hydrate and seafloor bottom simulating reflectors by vertical fluid expulsion: J. Geophys. Res., **97**, 7025–7041.

Hyndman, R., and Spence, G., 1992, A seismic study of methane hydrate marine bottom simulating reflectors: J. Geophys. Res., **97**, 6683–6698.

Katzman, R., Holbrook, W. S., and Paul, C. K., 1994, Combined vertical-incidence and wide-angle seismic study of a gas hydrate zone, Blake Ridge: J. Geophys. Res., **99**, 17975–17995.

Kvenvolden, K. A., and Barnard, L. A., 1983, Gas hydrates of the Blake Outer Ridge, Site 533, Deep Sea Drilling Project Leg 76: Initial Reports of the Deep Sea Drilling Project, **76**, 353–365.

Kvenvolden, K. A., and Barnard, L. A., 1983a, Hydrates of natural gas in continental margins: Am. Assoc. Pet. Geol. Mem., **34**, 631–640.

Kvenvolden, K., 1993, Gas hydrates – geological perspective and global change: Reviews of Geophysics, **31**, 173–187.

MacKay, M. E., Jarrard, R. D., Westbrook, G. K., and Hyndman, R. D., 1994, Origin of bottom-simulating reflectors : Geophysical evidence from the Cascadian accretionary prism: Geology, **22**, 459–462.

Mindlin, R. D., 1949, Compliance of elastic bodies in contact: Trans. ASME, **71**, A–259.

Murphy, W. F. I., 1982, Effects of microstructure and pore fluids on the accoustic properties of granular sedimentary materials: Ph.D. thesis, Stanford University.

Pearson, C., Murphy, J., and Hermes, R., 1986, Acoustic and resistivity measurements on rock samples containing tetrahydrofuran hydrates: J. Geophys. Research, **91**, 14132–14138.

Singh, S., Minshull, T. A., and Spence, G., 1993, Velocity structure of a gas hydrate reflector: Science, **260**, 204–207.

Stoll, R. D., and Bryan, G. M., 1979, Physical properties of sediments containing gas hydrates: J. Geophys. Research, **84**, 1629–1634.

Whalley, E., 1980, Speed of longitudinal sound in Clathrate hydrates: J. Geophys. Res., **85**, 2539–2542.